

Numerical and Experimental Study of the Performance of Electromagnetic Flowmeter in Annular Flow

Ihsaan Nadhum Jawaad
 Department of Mechanical Engineering
 University of Basrah
 College of Engineering

Muneer A. Ismael
 Department of Mechanical Engineering
 University of Basrah
 College of Engineering

Abstract- The present numerical and experimental work investigates the performance of electromagnetic flowmeter (EMF) for measuring the flow rate of annular flow. Adaptive finite difference technique is used for the numerical calculations and the experimental work is done by making some modification on an existing electromagnetic flowmeter and its testing rig. The performance of the modified EMF is evaluated using two criteria namely, the flowmeter sensitivity S and the conventional weight function non uniformity ϵ . These two criteria were checked against two parameters; thickness of flowing water (δ) and the electrodes angular position (θ_e). Experimentally, three different water thickness ($\delta/R_o = 0.216, 0.373, 0.218$) and three electrode position ($\theta_e = 0^\circ, 11.25^\circ, 45^\circ$) were studied. The theoretical and experimental results have showed that these devices work properly in the annular flow case, where the most suitable electrode position in the annular flow was found to be in the conventional position ($\theta_e = 0^\circ$).

Keywords: electromagnetic flowmeter, annular flow, adaptive finite difference

1. Introduction

Electromagnetic flowmeter (EMF) is one of the most accurate devices that are used in measurement of the electrically conducting liquids. Electromagnetic flowmeters are suitable for measuring a wide variety of liquids having a lower electrical conductivity equal to that of distilled water (4×10^{-6} S/m) [1]. The history of EMF may refer to Faraday (1832) when he developed his theory about electrical induction. The first EMF was built by Kolin [2] to measure the blood flow in blood vessels. Since, the studies about this subject was wide spread [3– 6]. A novel study on EMF was published by Al-Rabeh et al. [7] where they presented the theory that provides a basis for design of electromagnetic flowmeters for fluids with dielectric and magnetic properties and with low conductivity. Hemp [8] developed a numerical method for designing the magnetic field so as to reduce the effect of the velocity profile as well as the total flow rate on the reading of an electromagnetic flowmeter. The proposed numerical method led to improvements in the design of both industrial and medical flowmeters. Bevir et al. [9] described very elegant piece of work in which magnetic field measurements around the tube wall were used to compute the weight function. They concluded that sensitivities would be predicted for most flowmeters by their procedures with an error of not more than 0.5%. Luntta and Halttunen [10] computed a model for an electromagnetic flowmeter and the error in distorted flow. Their results showed that the error can be expected to be less than 0.5% if the distance between the disturbance and the meter is

more than $5D$. Katutis and Virbalis [11] investigated creating the battery –driven electromagnetic flowmeter for reduction of power consumption, the main attention was paid on reduction of excitation current of magnetic field. Some researchers focused their studies to investigate the modeling the magnetic field inside the flowmeter [12] and frequency excitation behavior of the magnet [13].

There are some situations where the flowing fluid doesn't fill the entire cross sectional area of the conduit. This means that there exist air-filled regions within the flowing liquid. Partially-filled pipes or free surface flow are examples of this flow [14-15]. Annular flow is an important flow regime in many industrial applications. Some applications are inherently to have annular flow passages (i.e. there is no gaseous core flow) as in aero-engines, turbo machinery and various chemical and medical industrial devices. Bernier and Brennen [16] investigated the use of an electromagnetic flowmeter for the two-phase flow. Their study was both theoretical and experimental. They concluded an important relation for EMF that the signal in two-phase flow is over estimate of that when the liquid fills whole the pipe. Wyatt [17] performed the sensitivity analysis of the electromagnetic flowmeter for two-phase flow conditions such as bubbly and annular flows. The pervious conclusions were argued of [17] were correct when the dispersed phase consists of uniformly distributed, small and randomly oriented bubbles, which creates a macroscopically uniform and isotropic suspension. A magnetic flowmeter was showed also applicable to ideal annular flow with an axisymmetric liquid flow field. Zhang [18] investigated theoretically the effect of the phase distribution on the rectilinear weight function in a two-dimensional annular domain with or without eccentricity, and proposed a new rectilinear weight function as a series solution. Cha et al [19] investigated the characteristics of an electromagnetic flowmeter in a liquid metal two-phase flow; AC electromagnetic flowmeters were designed and manufactured. The two-phase flow was realized experiments, encompassing bubbly to slug flow regimes with a water-air mixture and a liquid sodium-nitrogen mixture, respectively. In the case of a slug flow, the phase and the amplitude of the flowmeter output changed rapidly when a slug bubble passed through the flowmeter. Their experiments showed that the electromagnetic flowmeter is a useful device for identifying the flow regimes. Ahn et al [20] developed the theory of the electromagnetic flowmeter to sense the flow current rather than the induced voltage for a high temporal resolution for two-phase flow measurements. The flow pattern coefficients were evaluated for vertical annular flows with various film thicknesses. The output of the

flowmeter was showed depends on the liquid conductivity (sensitive to temperature) and flow configurations of the two-phase flow with sinusoidal excitation. To our best knowledge, the conventional EMF is not investigated with horizontal annular flow yet and the electrode position was also not studied with horizontal annular flow. This motivated us to do 3D, theoretical, and experimental study of electromagnetic flowmeter to test the performance of these devices with annular flow.

2. Theoretical Background

2.1 Governing equations

The conventional form of EMF is shown in Fig. 1, it consists of an electrically insulating cylindrical flow channel (about 3 diameters in length) of circular cross-sectional, in the wall of which two small diametrically opposed electrodes are fitted, their surfaces in contact with the flowing liquid. A suitable external magnetic field is imposed perpendicular to both channel axis and the diameter line joining the two electrodes. An electric potential is produced by the movement of the liquid. The electric potential is picked up by the electrodes, amplified and recorded as a measure of the flow rate through the channel. The theoretical expression of the induced potential is given by Bevir [5] as a volume integral of the dot product of the liquid velocity vector \mathbf{v} and a weight vector \mathbf{W} as follow:

$$\Delta U = \int_{\tau} \mathbf{v} \cdot \mathbf{W} d\tau \quad (1)$$

Where \mathbf{W} is given by:

$$\mathbf{W} = \mathbf{B} \times \mathbf{J} \quad (2)$$

Here \mathbf{B} is the magnetic field vector and \mathbf{J} is the virtual current vector (hypothetically, \mathbf{J} is the current density that is defined as the unit current that moves between two electrodes with no liquid motion [5]). τ is the effective flowmeter volume, by effective it is meant the volume at its two ends, both \mathbf{B} and \mathbf{J} are decay to zero. The main drawback of this flowmeter is that the output signal may be sensitive to any changes in the velocity profile for the same amount of flowrate. The degree of flowmeter influence by the velocity variation is conventionally evaluated depending on the z-component of the weight vector, where in most applications, the flow is assumed to be rectilinear i.e. $\mathbf{v} = v_z$, $v_r = v_{\theta} = 0$, then the integral of equation (1) is approximated to:

$$\Delta U = \int_0^{2\pi} \int_0^{R_0} W_{zi}(r, \theta) v_z(r, \theta) r dr d\theta \quad (3)$$

Where R_0 is the internal channel radius and $W_{zi}(r, \theta)$ is the integrated rectilinear weight function along the flowmeter effective axis;

$$W_{zi}(r, \theta) = \int_{-\infty}^{+\infty} W_z(r, \theta, z) dz \quad (4)$$

Examining the parameters of the integral of equation (3), it is possible to make the flowmeter signal as a function to the flow rate only by extracting $W_{zi}(r, \theta)$ out of the integral sign i.e. making it constant through the flowmeter cross-sectional area.

2.2 Performance Criteria

i- Weight function non-uniformity

The most common used criterion of the weight function distribution is the weight function non-uniformity ϵ criterion which has been formulated by Hemp [8]:

$$\epsilon = \frac{1}{A} \int_A \left| 1 - \frac{W_{zi}(r, \theta)}{\overline{W_{zi}(r, \theta)}} \right| dA \quad (5)$$

$\overline{W_{zi}(r, \theta)}$ is the average of the rectilinear weight function over the flow cross section area;

$$\overline{W_{zi}(r, \theta)} = \frac{1}{A} \int_A W_{zi}(r, \theta, z) dA \quad (6)$$

The minimum value of the ϵ is the best the flowmeter design from the sensitivity to variations in the velocity distribution point of view. For an "ideal" flowmeter, the weight function is uniform and the value of this criterion is zero.

ii- Sensitivity

The other performance criterion is the sensitivity measure S which gives the strength of the flowmeter output (ΔU) compared with that of Shercliff [3] output ($BDVm$), hence:

$$S = \frac{\Delta U}{BDVm} \quad (7)$$

Where; ΔU here is of equation (3), D is the flowmeter diameter, and Vm is the mean velocity of the metered liquid. This criterion represents also the flow signal in a dimensionless quantity, not affected by flowmeter dimensions and flow rate.

2.3 Numerical Solution

The calculation of \mathbf{W} is carried out by solving \mathbf{J} and \mathbf{B} in same lattice points of the numerical solution mesh. The present numerical solution was achieved using an efficient adaptive finite differences approach that refines the mesh at necessary regions, the details of this approach are given in [15]. However, In the case of uniform electrical conductivity, \mathbf{J} is expressed as;

$$\mathbf{J} = -\nabla G$$

Which is possible as $\nabla \times \mathbf{J} = 0$ (Maxwell's equation) and then G is found by solving Laplacian operator of G in cylindrical coordinates with its appropriate boundary conditions;

$$\nabla^2 G = 0 = \frac{1}{r} \frac{\partial G}{\partial r} + \frac{\partial^2 G}{\partial r^2} + \frac{\partial^2 G}{\partial z^2} + \frac{1}{r^2} \frac{\partial^2 G}{\partial \theta^2} \quad (8)$$

Due to \mathbf{B} , assuming that the applied magnetic field is unaffected by the 'small' induced current, thus;

$\mathbf{B} = -\nabla F$, and F is found as in G (for a given magnetic field geometry)

$$\nabla^2 F = \frac{\partial^2 F}{\partial r^2} + \frac{1}{r} \frac{\partial F}{\partial r} + \frac{1}{r^2} \frac{\partial^2 F}{\partial \theta^2} + \frac{\partial^2 F}{\partial z^2} \quad (9)$$

Discretizing each term of Eqs. (8) and (9), the G and F formulas can be written as:

$$G_i = \frac{1}{S_i} \left\{ \begin{aligned} & \left(\frac{1}{S_1(S_1+S_2)} + \frac{1}{2r(S_1+S_2)} \right) G(\text{no}(i)) + \\ & \left(\frac{1}{S_2(S_1+S_2)} - \frac{1}{2r(S_1+S_2)} \right) G(\text{so}(i)) + \\ & \frac{1}{r^2} \left(\frac{1}{S_3(S_3+S_4)} \right) G(\text{we}(i)) + \frac{1}{r^2} \left(\frac{1}{S_4(S_3+S_4)} \right) G(\text{es}(i)) + \\ & \left(\frac{1}{S_5(S_5+S_6)} \right) G(\text{fr}(i)) + \left(\frac{1}{S_6(S_5+S_6)} \right) G(\text{ba}(i)) \end{aligned} \right\} \quad (10)$$

where:

$$S_i = \left[\begin{aligned} & \frac{1}{s_1(s_1+s_2)} + \frac{1}{s_2(s_1+s_2)} + \frac{1}{r^2} \left(\frac{1}{s_3(s_3+s_4)} + \frac{1}{s_4(s_3+s_4)} \right) + \\ & \frac{1}{s_5(s_5+s_6)} + \frac{1}{s_6(s_5+s_6)} \end{aligned} \right] \quad (11)$$

The formula of F_i is as same as that of eq. (10) but by replacing each G by F , it is not shown here for brevity. By referring to Fig. 2, the notations *no*, *so*, *we*, *es*, *fr*, *ba* denote to north, south, west, east, front and back, respectively, of the node i and S is the interval as shown in Fig. 2. Due to symmetry (see Fig. 3a), one-fourth of the entire geometry can be solved numerically; this will save computational efforts and increase the accuracy of the numerical solution. The boundary conditions of G are as follow (see Fig. 3b):

1) $G = \text{constant}$ on the electrode and it is set to be unity ($G = 1$).

2) $G = 0$ at the end of the flowmeter (at $z = L$).

3) $\frac{\partial G}{\partial z} = 0$ at $z = L/2$ (in the electrodes plane) due to symmetry.

4) $\frac{\partial G}{\partial n} = 0$ at the flowmeter tube ($r = R_o$) and the inner

cylinder surface ($r = R_{\text{gas}}$). In this case,

$$\frac{\partial G}{\partial n} = \frac{\partial G}{\partial r} \Big|_{r=R_o} = \frac{\partial G}{\partial r} \Big|_{r=R_{\text{gas}}} = 0$$

On the other hand, the boundary conditions of F (see Fig. 4) are written as [15]:

1) $F = f_1(\theta)$ at the upper pole piece and $F = f_2(\theta)$ on the lower pole piece. Where $f_1(\theta) = -f_2(\theta)$ were calculated in [15].

2) $F = 0$ at the liner wall, the curved surface ABCD except the two magnet pole pieces.

3) $\frac{\partial F}{\partial \theta} = 0$ at the plane surface ABCD due to symmetry.

4) $\frac{\partial F}{\partial z} = 0$ due to symmetry at $z = L/2$ for annular flow case.

5) $F = 0$ at the $z = L$, this plane is far from magnet center.

The criterion of choosing nodes to be refined is that the local error (Er) of these nodes exceeds or equals to a predetermined error. This predetermined error is termed as critical error and calculated as [21]:

$$e_{\text{crit}} = e_{\text{max}} - \beta(e_{\text{max}} - e_{\text{min}}) \quad (12)$$

Hence the criterion is:

$$Er \geq e_{\text{crit}} \quad (13)$$

Where, e_{crit} is the critical (predetermined) error, e_{max} is the maximum error, e_{min} is the minimum error and β is a selectable factor, $0 < \beta < 1.0$. If any node is marked to be refined, or in other words to be source of refinement, three new nodes are added, one in each direction. The position of each new added node is mid-distance between the marked node and its neighbor one. In order to avoid the ill-conditioning meshes, a limit for the distance between the nodes is used as a second parameter (d_{min}) of the h-adaptive method [22], in such a way that if the distance between the new added node and its neighbor is smaller than this minimum distance (d_{min}), then the new node should not be added. The minimum distance is calculated as;

$$d_{\text{min}} = \gamma * d_{\text{max}} \quad (14)$$

Where $0 < \gamma < 1$, and d_{max} is the maximum distance between any two nodes in the initial coarse mesh such that;

$d_{\text{max}} = \Delta r$ in r direction ,

$d_{\text{max}} = \Delta \theta$ in θ direction ,

$d_{\text{max}} = \Delta z$ in z direction

where Δr , $\Delta \theta$ and Δz are respectively; the radial; azimuthally, and axial intervals of the initial coarse mesh.

However, the numerical efforts which were achieved by FORTRAN can be summarized as in Appendix 1.

3. Experimental work

The evaluation procedure of electromagnetic flowmeter performance is usually enhanced by real calibration in a flowmeters testing rig. So that it was decided to experimentally test the annular flow EMF performance. The matter which encouraged us to do the experiments is that a laboratory EMF together with a flowmeter testing rig are already exist in the laboratory of fluid mechanics in Mech. Eng. Dep. in Engineering college of Basrah University. But the existing testing rig is designed to generate fully-filled and partially-filled flows. Therefore, an adaptation was made on this testing rig to handle the annular flow test.

3.1 Description of the Laboratory EMF

The construction of the existing laboratory EMF is composed of two main elements, namely the primary and secondary elements. The primary element composed of:

i- The flowmeter tube (PVC 67 mm inner diameter, 4.2 mm thickness and 210 mm long) which is electrically insulating and magnetically permeable.

ii- Three pairs of point electrodes (3.2 mm diameter, stainless steel 316-L) each pair fixed at 0° , 11.25° and 45° with flowmeter horizontal axis.

iii- Magnetic field generator, which is a modified iron yoke wounded in such a way to act as a north and south poles. It is driven by 50 Hz AC sine wave power source.

iv- Two aluminum flanges and two longitudinal studs to clamp the flowmeter tube and to enable the connection with the flow circuit. Figure 5 shows schematically the primary element which is sometimes called "transmitter".

The secondary element which is sometimes called (receiver) is an electronic circuit composed of a set of operational amplifiers, resistors, capacitors and one electronic switch. The function of this circuit is to extract and amplify the flow signal from other noise signals.

3.2 Description of the Test Rig

The flowmeter testing rig existing in the laboratory of fluid mechanics is closed cycle of tap water. It consists of two in-plane reservoirs ($0.8 \times 0.8 \times 1$ m³ capacity for each) connected by two pipes (lower Galvanized Steel and upper PVC). A one horsepower centrifugal pump (1" \times 1") is installed in the lower (1" ID) pipe to circulate the flow through the upper (67 mm ID) PVC pipe. It sucks water from the left reservoir 1 and pumped it into the right reservoir 2, the quantity of water is controlled by a gate valve fixed at the pump discharge section. After the water level in the right reservoir 2 increases, the flow in the upper pipe is induced hydrostatically. Flowmeter under test is flanged in the upper pipe in such a position to perform free lengths of 14D and 13D up and downstream of the flowmeter respectively. Also there are two transparency sections in the upper pipe. The flow rate through the upper pipe is controlled by a gate valve fixed at the end of the upper pipe. But in some flow values, the valve existing in the pump discharge is shared to control the flow rate in the upper pipe. More descriptions of this flowmeter testing rig are given in [15]. This rig is designed to run fully-filled or partially-filled of plane free surface. So that, some modifications were achieved in the present study to handle annular flow. Inducing a two phase annular flow is impossible in the present test rig, as this flow occurs in the very high velocities and may requires compressing an air jet through the pipe center. Nevertheless, it is possible to adapt this flow rig to carry out annulus flow i.e. a flow between two concentric cylinders. Hence, the main modification on the test rig is to insert, coaxially, an inner solid cylinder into the main flowmeter pipe (outer pipe, as will be called henceforth). Three inner cylinders of different diameters (25, 42, 50.4 mm) were selected; each one has a length of 1.25 m (L_c). They are made from a PVC pipes because of the PVC pipe is electrically insulating (to prevent the short circuit of the generated signal) and magnetically permeable (to avoid the distortion of the applied magnetic field), each one of these cylinders

was tested separately by fixing it from its two ends. The position of the inner cylinder inside the outer pipe was set in such a way that the laboratory flowmeter acts on the mid span of the annulus flow. Accordingly, the free up-and downstream lengths available are similar and equal to 9D with respect to the flowmeter. These free lengths are quite enough to verify fully developed flow through the annulus. The mechanism of fixing the inner cylinder inside the outer pipe was achieved as followings (Fig. 6):

1-Making two holes ($L_s=1.05$ m) apart through the top surface of the upper pipe and inserting a threaded sleeve in each hole.

2-Making two holes in the inner cylinder, to be opposite to that holes in the outer pipe.

3-After entering the inner cylinder inside the outer pipe, two screws are threaded, in each sleeve. These screws were selected to be as thin as possible to avoid the disturbance of the flow passage. By the virtue of the visualization of the transparency two sections available in the upper pipe line, these two screws and after fixing their ends with the inner cylinder, are used to adjust the inner cylinder position for reaching the concentric annulus. Then, the two threaded sleeves are filled by resin to prevent water leakage. Fig. 6 illustrates this process and Fig. 7 illustrates the test rig after modification. The steps 2-3 are repeated for each one of the three inner cylinders. The inner cylinder is entered inside the outer pipe by removing some fitting parts existing there. Fig. 8 displays the photo of the entire annular flow test rig.

4. Results and discussion

The numerical and experimental results are presented in this section. It is necessary to check the validity of the numerical solution procedure followed in this work. Because of the present numerical procedure is adaptively refine the mesh and the adaptation range could be controlled by imposed critical error e_{crit} eq. (12), so that the flowmeter characteristics (S and ε) are checked with a number of domain grids. Accordingly, it was seen that the results stabilize when β factor lies between (0.6-0.8). Therefore, a value of $\beta = 0.6$ was chosen to be based on throughout the numerical results as it economic from the computational time point of view.

4.1 Theoretical Results

The contours of rectilinear weight function and the flowmeter criteria S and ε are tested numerically for electrode position $\theta_e = 0 - 45^\circ$ with fine intervals, and gas to liquid ration $\delta/R_o = 0.1 - 0.8$. The weight function distribution (contours) shown in Fig. 9 and Fig. 10 are calculated as integrated weight function along z axis and normalized by integrated weight function at the electrode. Figure 9, for example explain the effect of lowering the position of the electrode on the distribution of weight function over the flowmeter cross-sectional area, where a clear symmetric appears when $\theta_e=0^\circ$ (Fig. 9a). This symmetric is lost gradually with lowering the electrode position (increasing θ_e) as shown in Fig. 9b where the strength of weight function is localized in the lower half of flowmeter cross-sectional area, while the upper half seems to be very weak. Fig. 10 also shows this effect but for different liquid thickness. In Fig. 10, the liquid thickness

($\delta=0.373 R_o$ and its equal to 25 mm) is less than that of Fig. 9 ($\delta=0.627 R_o$ and its equal to 42 mm) A comparison between these two figures clarifies the effect of reducing the passages of virtual current on the magnitude of the weight function, where for same electrode position and at the effective regions, the values of the normalized weight function are larger at smaller liquid thickness because of increasing the strength of the virtual current.

The sensitivity of flowmeter for annular case is shown in Fig. 11 for different liquid thicknesses and three electrode positions ($\theta_e=0^\circ, 11.25^\circ, 45^\circ$). Only these three electrode positions were considered here because of the experimental laboratory flowmeter contains this electrode arrangement. This figure shows that when the liquid thickness (δ) decreases, the flowmeter sensitivity decreases. Since the magnetic field doesn't affected by the void region, this behavior is attributed to the virtual current only. Since the virtual current doesn't pass through the void, hence, increasing the void regions (decreasing δ) leads to decrease of the virtual current passages of electrically conducting liquid. The effect of electrode position seems to be less. Nevertheless, the behavior against electrode position can be extinguished according to the flowing liquid thickness. For $\theta_e=0$ and $\theta_e=45^\circ$, and when liquid thickness less than $0.5R_o$, the flowmeter sensitivitty S increases with increasing θ_e and vice versa when liquid thickness is larger than $0.5R_o$. It is noticed that when $\theta_e=11.25^\circ$, largest values of S are recorded. This behavior is attributed to that when θ_e decreases, the current stagnation points are decreased where the stagnation points become more effect when $\theta_e=0^\circ$, provided that the annular liquid thickness is regular i.e. concentric cylinders.

The weight function non-uniformity criterion ε is depicted in Fig. 12. It can be seen from this figure that the non-uniformity of the weight function increases with decreasing the thickness of the flowing liquid. This is attributed to that when the void is increased, the passages of virtual current is contracted resulting in generation of regions of high localized current values. These regions lead to increasing the non-uniformity of the weight function through the flowmeter section. The electrode positions $\theta_e=0^\circ$ and $\theta_e=11.25^\circ$ are more affected by the liquid thickness variation than other positions.

4.2 Experimental Results

The experimental results are drawn from testing a combinations of three annular water thickness ($\delta/R_o = 0.627, 0.373, 0.218$) and three electrode positions ($\theta_e = 0^\circ, 11.25^\circ, 45^\circ$). This results in nine calibration curves. These calibration curves were achieved between the actual volumetric flow rate through the flowmeter (on x-axis) and the experimental and theoretical outputs (on y-axis). The actual flow rate was measured by classical (but still the most accurate) stop watch and Baker i.e. measuring the time required to filling a specified volume of water outlet from the upper pipe and entering Reservoir 1. The theoretical output was calculated by inserting the average water velocity in fully developed region (obtained from dividing the measured flow rate by the annular cross-sectional area) in to the FORTRAN 77 program which

calculate the theoretical flowmeter output signal. Relation of best fit was edited on each one of the calibration curves for experimental data and the theoretical data (Figs. 13-15). The theoretical relation is a pure slope of linear line, while the experimental relation involves an intercept value which represents the reading of flowmeter despite zero flow rate (zero reading). This zero reading refers to some shift in the electronic detection circuit. The slope in both relations (experimental and theoretical) represents the device sensitivity which is common in measurement and instrumentation fields namely the output/input ratio.

Except the case of $\theta_e=11.25^\circ, \delta=0.373 R_o=25$ mm a noticeable discrepancy between the theoretical and experimental slopes could be clearly extinguished from the calibration curves and also from Table 1 where the whole slopes and the percentage error between the experimental and theoretical slopes for each case are reported. From this table and remembering that the sensitivity values listed in it represent the (output/input) ratio. As stated previously, these device, are designed to be flow rather than velocity meters, so that, the output is set to be as flow rate in liters per second. Accordingly, the optimum performance is specified when the output signal (in millivolts) is constant at different annulus areas for the same flow rate. The contents of Table 1 do not be so, where it is clear that the output is influenced by the annular cross-sectional area. The uncertainty in positioning of the inner cylinder to be coaxially with the origin flowmeter tube, prescription of the components of the electronic detection circuit, and uncertainty regarding with the instrumentation of recording the flow rate are some reasons causing the high discrepancy between the theoretical and experimental results. However, the electrode position is not so important because of any flowmeter works with one selected electrodes pair (at a specified position). Moreover, the output linear relation is still hold in these devices with annular flow. However, an attention on designing the electromagnetic flowmeter must be introduced when used in measurement of annular flow.

5. Conclusions

The numerically and experimentally study of the performance of electromagnetic flowmeter for annular flow case led to the following conclusions:

- 1- The obtained results have demonstrated that the ability of electromagnetic flowmeters to measure the rate of annular flow.
- 2- The optimum position of the pick-up electrodes is found to be as same as that in conventional electromagnetic flowmeters i.e. at $\theta_e = 0$
- 3- The excepted error due to changes in the annular velocity profiles is larger for thinner thickness of the flowing liquid. This is because the recorded higher values of ε at lower thickness of the metered liquid.
- 4- The sensitivity S increases slightly with liquid thickness (δ).

APPENDIX 1 Steps of Adaptive Finite Difference Solution

- i-Read the number of divisions of the initial mesh together with the domain dimensions (N_r , N_θ , N_z are the radial; azimuthally, and axial respectively divisions) and generate the initial coarse mesh.
- ii-Solve F and G at initial coarse mesh
- iii-Calculate the maximum error at each node for both F and G domains.
- iv-Calculate the critical error (ϵ_{crit}) and compare it with the maximum error.
- v-Cluster the nodes that verified the critical condition (to be refined).
- vi-Add three new nodes (one node in each coordinate) for each clustered node of the initial coarse mesh.
- vii-Calculate the potential (F or G) of each added node, by adding additional nodes at the neighbor area.
- viii-Repeat step ii but for the new fined mesh
- ix-Repeat steps ii to viii until the imposed accuracy is attained.

6. References

- [1] Baker R. C. "Flow Measurements Handbook, Industrial Design, Operating Principles, Performance and Applications" Cambridge U.K. Cambridge University Press, 2000.
- [2] Kolin A., "An electromagnetic flowmeter, the principle of the method and its application to blood flow measurement," PWC. Sac. Exptl. Biol., vol. 35, 1936, pp. 53-57.
- [3] Shercliff J, A, "Relation between the velocity profile and the sensitivity of electromagnetic flowmeter" J. Appl. Phys. Vol. 25, 1954, pp 817-818.
- [4] Cushing V., "Induction flowmeter", Rev. Sci. Instrum. vol. 17, 1958, pp 488-503.
- [5] Bevir M. K., "The theory of induced voltage of electromagnetic flowmeters". J. Fluid Mech., vol. 43, 1970, pp 577-590.
- [6] Baker R., C, "Numerical analysis of the electromagnetic flow measurement". Procc. IEE. Vol. 120, No.9, 1973, pp. 1089-1043.
- [7] Al-Rabeh R. H., Baker R. C. and Hemp J., "Induction flowmeter for poorly conductive fluids" Proc. Royal. Society. Lond. A 361, 1978, pp. 93-107.
- [8] Hemp J., "Improved magnetic field for an electromagnetic flowmeter with point electrodes" J. phys. D: Appl. Phys. Vol. 8, 1975, pp. 983-1002.
- [9] Bevir M. K., O'sullivan V. T. and Wyatt D. G., "Computation of electromagnetic flowmeter characteristics from magnetic field data", J. phys. D: Appl. phys., vol. 14, 1981, pp. 373-388.
- [10] Luntta. E. and Halttunen. J, "The Effect of Velocity Profile on Electromagnetic Flow Measurement", Sensors and Actuators, vol. 16, 1989, pp. 335 – 344.
- [11] Katutis R. and Virbalis J.A., "Development of battery-driven electromagnetic flow converter", Electronics and Electrical Engineering, No. 4, 2007, pp. 79-82.
- [12] Vijay Sharma, G.Vijaya Kumar, S.K. Dash, B.K. Nashine, K.K. Rajan, Modeling of Permanent Magnet Flowmeter for Voltage Signal Estimation and its Experimental Verification, Flow Measurement and Instrumentation, Vol. 28, (2012) 22-27
- [13] Tiejun Liu, Tongsheng Gong, Yinjia Chen, Development of an Electromagnetic Flowmeter with Dual Frequency Excitation, TELKOMNIKA, Vol.10, No.8, December 2012, pp. 2013-2019
- [14] [13] Wei Kaixia, Haoshurong, The design of Electromagnetic flowmeter in partially filled pipes, Applied Mechanics and materials Vols. 130-134 (2012) pp 1357-1360
- [15] Ismael M.A., "Numerical and experimental studies of electromagnetic flowmeter for partially-filled pipes" Ph.D. Thesis, University of Basrah, 2007.
- [16] Bernier R. N. and Brennen C. E., "Use of the electromagnetic flowmeter in a two-phase flow" Int. J. Multiphase flow Vol. 9 No. 3, 1983, pp. 251-257.
- [17] Wyatt D. G., "Electromagnetic flow meter sensitivity with two phase flow. International Journal of Multiphase Flow", vol. 12, No. 6, 1986, pp. 1009–1017.
- [18] Zhang X. Z., "The effect of the phase distribution on the weight function on an electromagnetic flowmeter in 2D and in the annular domain" Meas. Sci. Technol. Vol. 8, 1997, pp. 1285-1288.
- [19] Cha J. E., Ahn Y. C. and Kim M. H. "Flow measurement with electromagnetic flowmeter in two-phase bubbly and slug flow regimes" Flow Measurement and Instrumentations Vol. 12, 2002, pp. 329-339.
- [20] Ahn Y. C. Oh B. D. and Kim M. H., " A current-sensing electromagnetic flowmeter for two-phase flow and numerical simulation of the three-dimensional virtual potential distribution: I. Fundamentals and annular flow" Meas. Sci. Technol. vol. 14, 2003, pp, 239-250.
- [21] Tristano J.R., Chen Z., Hancq D.A., Kowk W. "Fully automatic adaptive mesh refinement integrated into the solution process" ANSYS incorporated, Canonsburg, PA U.S.A
- [22] Urena F., Benito J.J., and Alvarez R. "Computational error approximation and h-adaptive algorithm for 3-D generalized finite difference method" International Journal for Computational Methods in Engineering Science and Mechanics. Vol. 6, 2005, pp. 31-39.

Notations			R_o	Flowmeter inner radius	m
\mathbf{B}	Magnetic field vector	Tesla	R_{gas}	Radius of inner cylinder	m
d_{max}	maximum distance between any two nodes	-	S	Flowmeter sensitivity criterion	-
d_{min}	minimum distance between any two nodes	-	\mathbf{v}	Liquid velocity vector	
e_{crit}	Critical error criterion	-	$V(r)$	liquid velocity at specific radius (r)	
e_{max}	Max. error in the solution mesh	-	$v(r,\theta)$	Rectilinear velocity distribution	
e_{min}	Min. Error in the solution mesh	-	$W_{zi}(r,\theta,z)$	Rectilinear weight function	$V.s/m^3$
Er	Local error	-	$\bar{W}_{zi}(r,\theta)$	Average of $W_{zi}(r,\theta,z)$	$V.s/m^3$
F	Magnetic field scalar potential	Tesla/m	β	Selectable factor for the e_{crit} criterion	-
G	Virtual current scalar potential	1/m	γ	Selectable factor for the d_{min} criterion	-
f_1, f_2	Functions of optimum F	-	δ	Annulus thickness of flowing liquid	m
\mathbf{J}	Virtual current density vector	A/m ²	ϵ	Criterion of the weight function non-uniformity	-
L_c	Length of the inner cylinder	m	θ	Angle measured from the magnetic field centre.	deg.
L	Length of conductor passing across a magnetic field or the flowmeter length	m	θ_e	Angular electrode position	deg.

Table 1: comparison between the theoretical and experimental slopes and the corresponding error

θ_e	δ / R_o	Theoretical slope	Experimental slope	Error %
0°	0.218	2.943	2.35	20.1
	0.373	1.96	2.836	45
	0.627	1.462	2.35	60.7
11.25°	0.218	3.156	2.326	26.3
	0.373	2.09	2.084	0.29
	0.627	1.54	2.117	37.5
45°	0.218	3.01	3.25	8
	0.373	1.98	2.252	14
	0.627	1.45	2.296	58.3

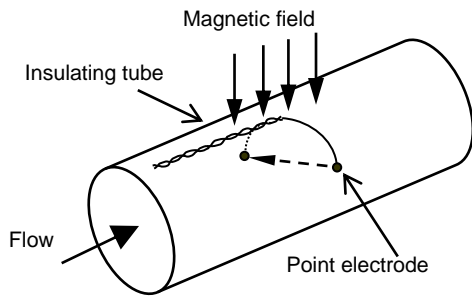


Fig.1 Principle of conventional electromagnetic flowmeter

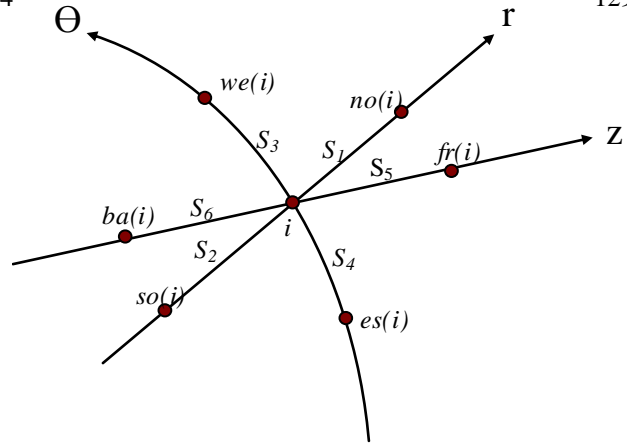


Fig. 2 Cylindrical coordinates notations of the numerical solution

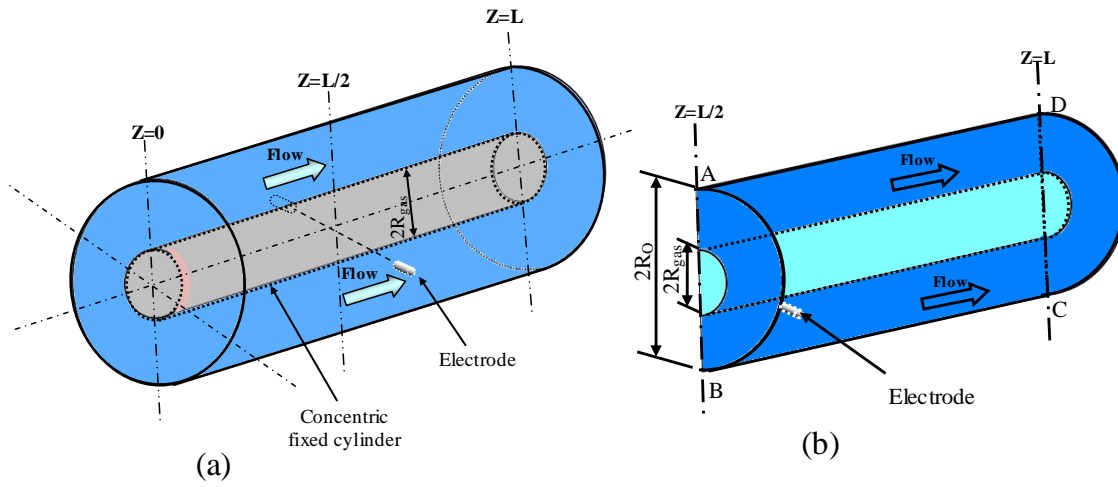


Fig. 3 Annular flow geometry (a) full pipe (b) one-fourth of the flow meter

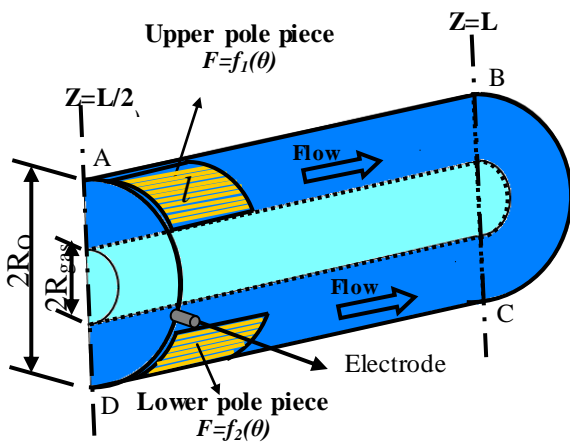


Fig. 4 one-fourth of the flow meter, F boundary conditions

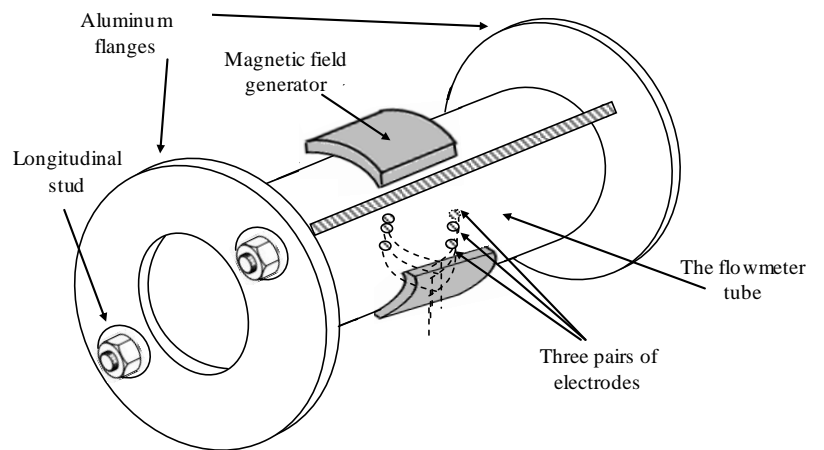


Fig. 5 Schematic of primary element components of EMF

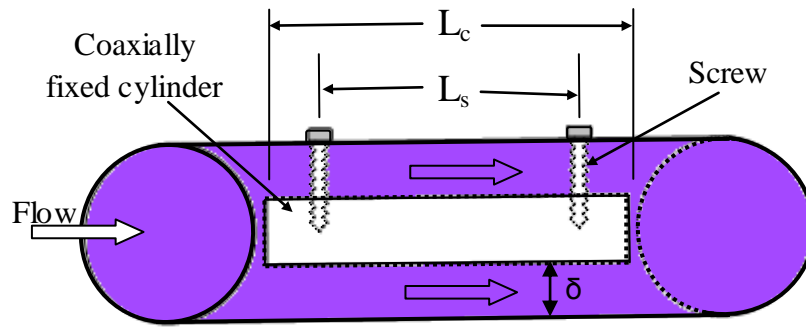


Fig. 6 Mechanism of making annulus flow

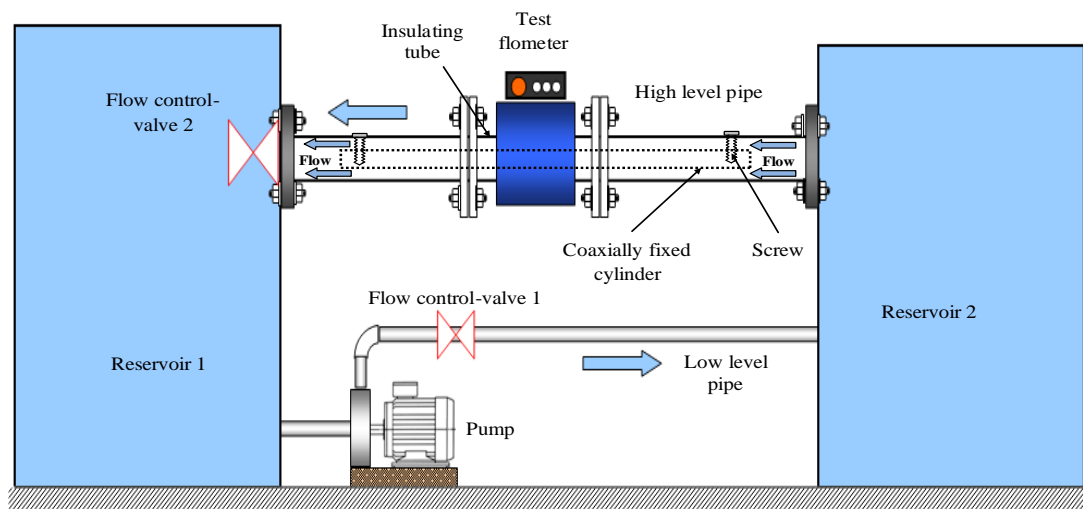


Fig. 7 Flowmeter test rig after modification

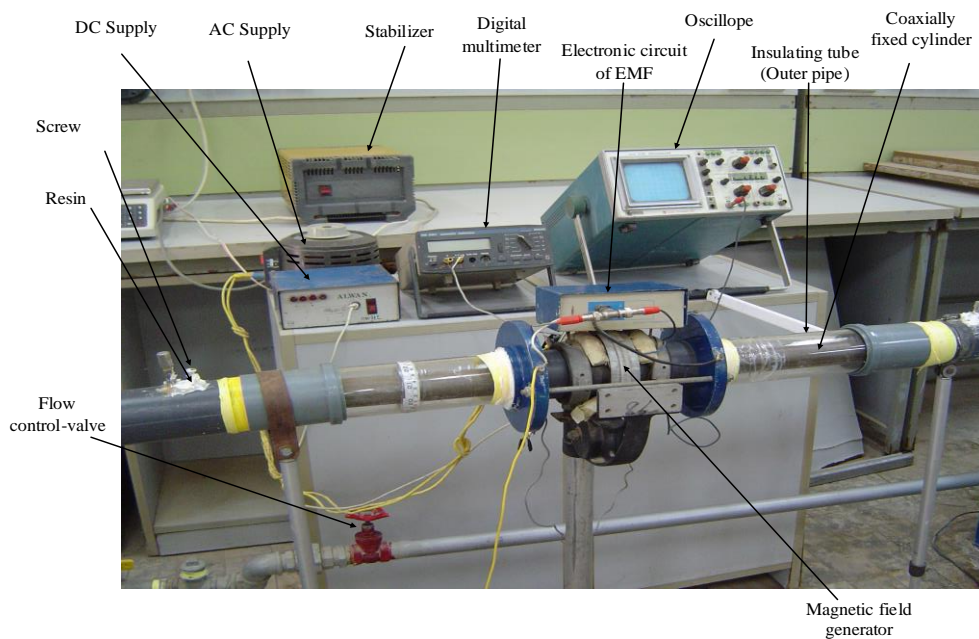


Fig. 8 Photo shows flowmeter test rig after modification

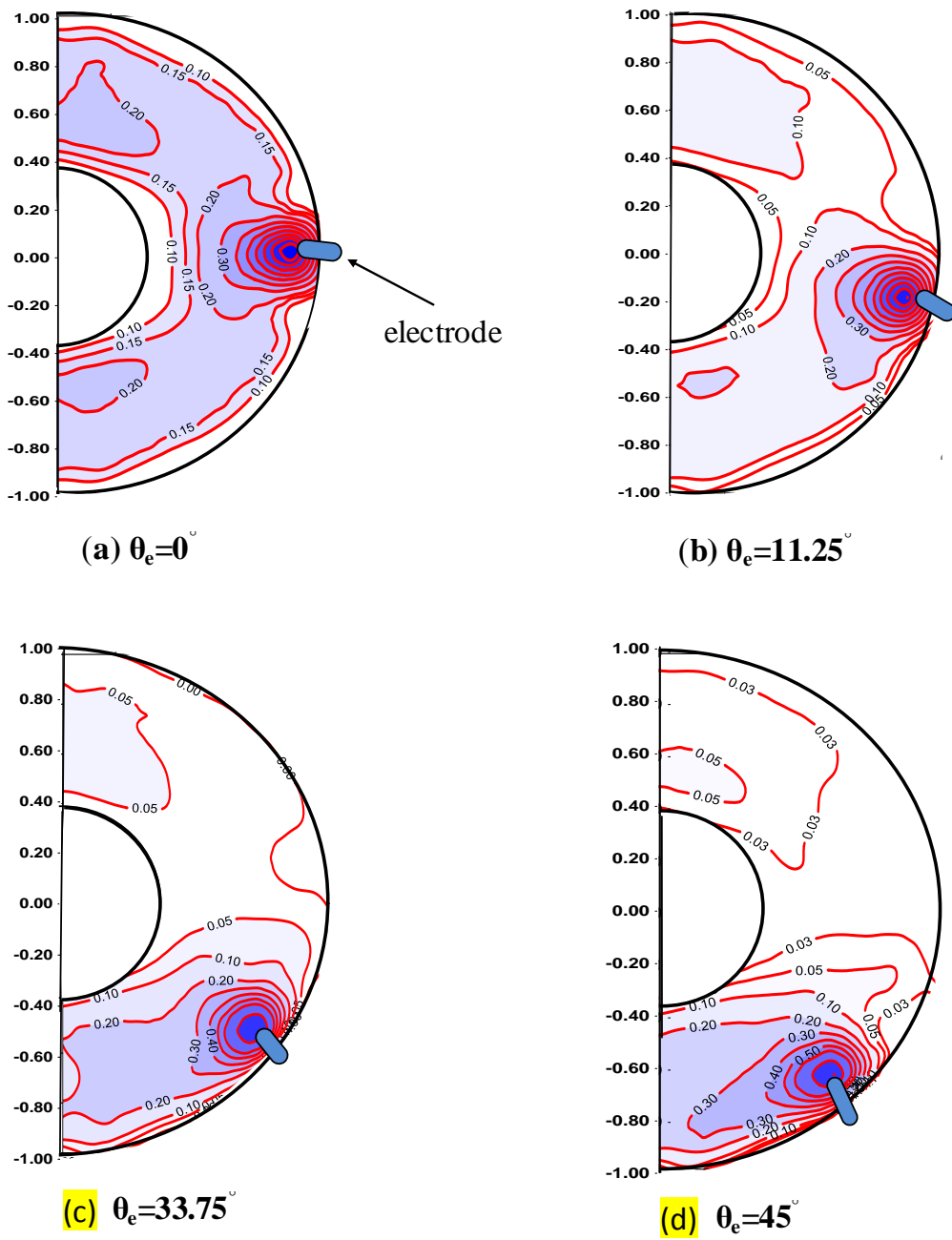


Fig 9 Integrated weight function contours for annular flow, $\delta=0.627 R_o$ at electrodes (a) $\theta_e=0^\circ$, (b) $\theta_e=11.25^\circ$, (c) $\theta_e=33.75^\circ$, (d) $\theta_e=45^\circ$

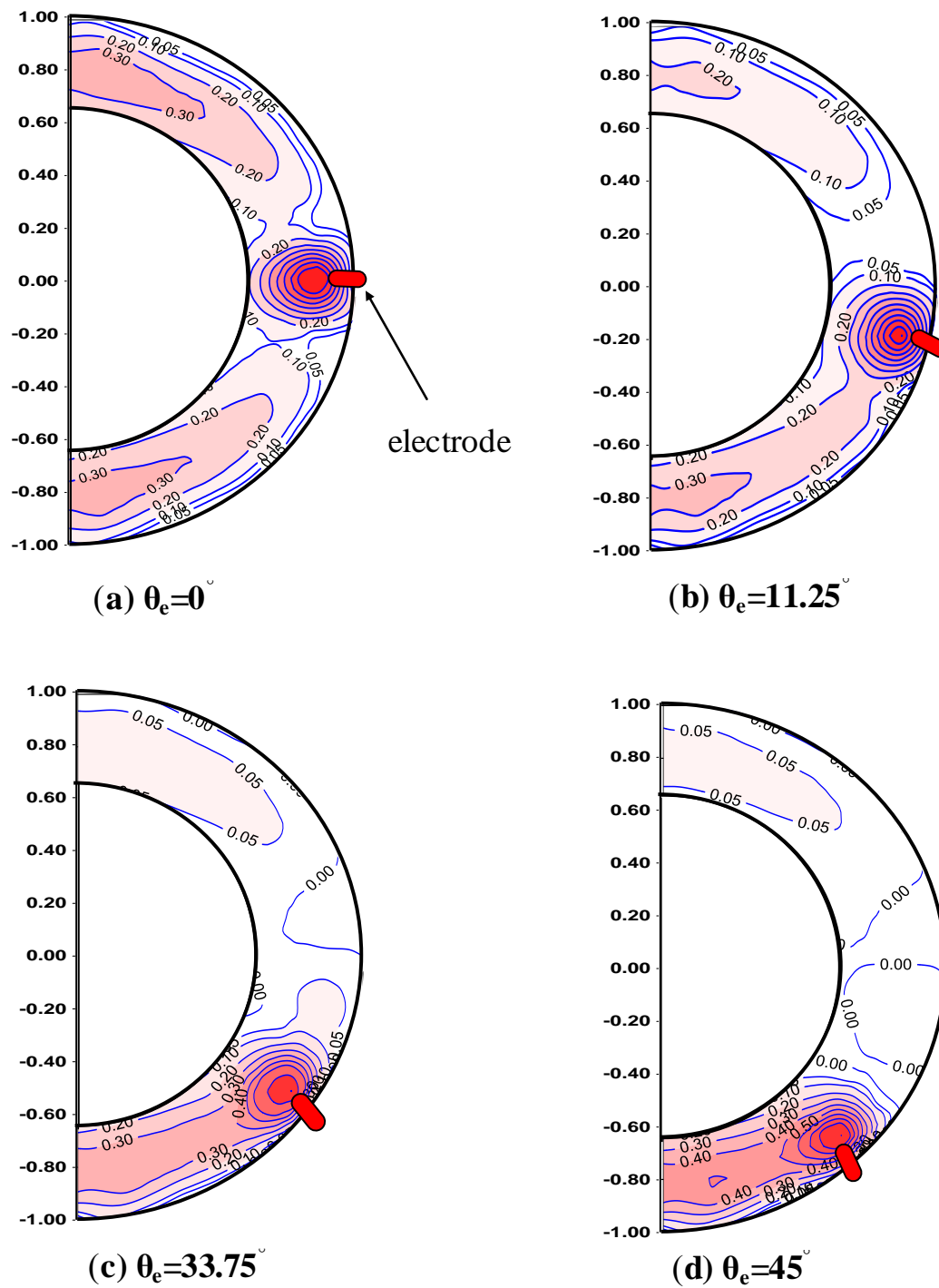


Fig. 10 Integrated weight function contours for annular flow, $\delta=0.373 R_0$ at electrodes, (a) $\theta_e=0^\circ$, (b) $\theta_e=11.25^\circ$, (c) $\theta_e=33.75^\circ$, (d) $\theta_e=45^\circ$

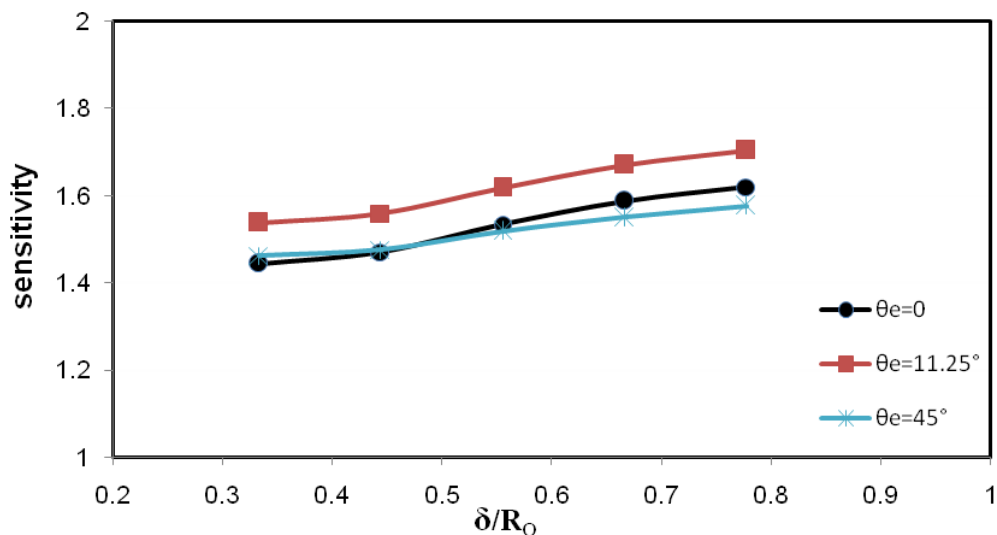


Fig. (11) Variation of sensitivity with the gas thickness for different electrode angular position

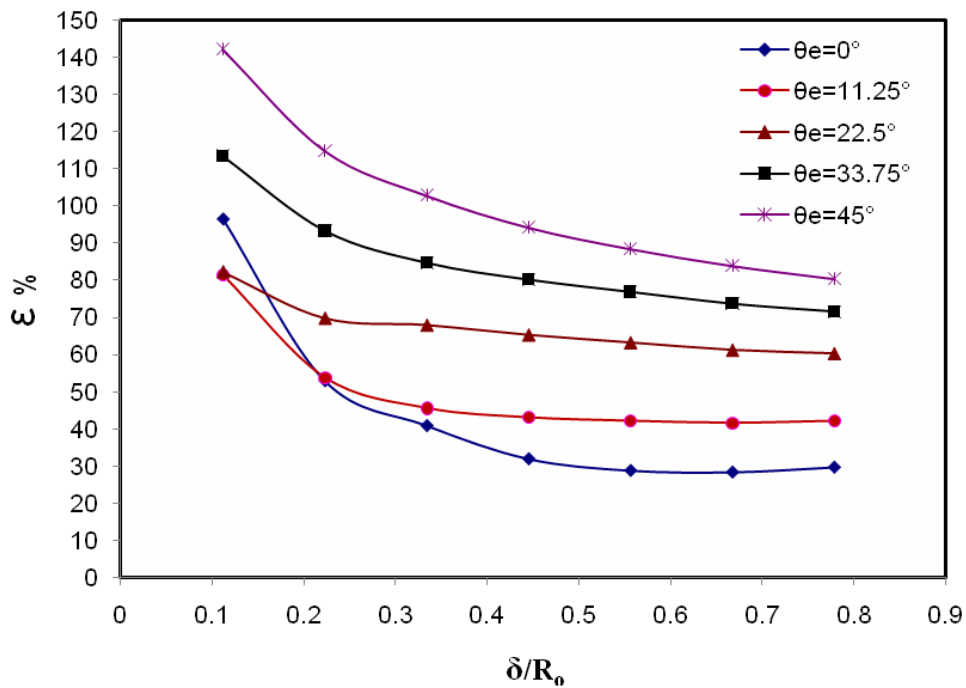


Fig. 12 Variation of weight function non-uniformity with the gas thickness for different electrode angular position

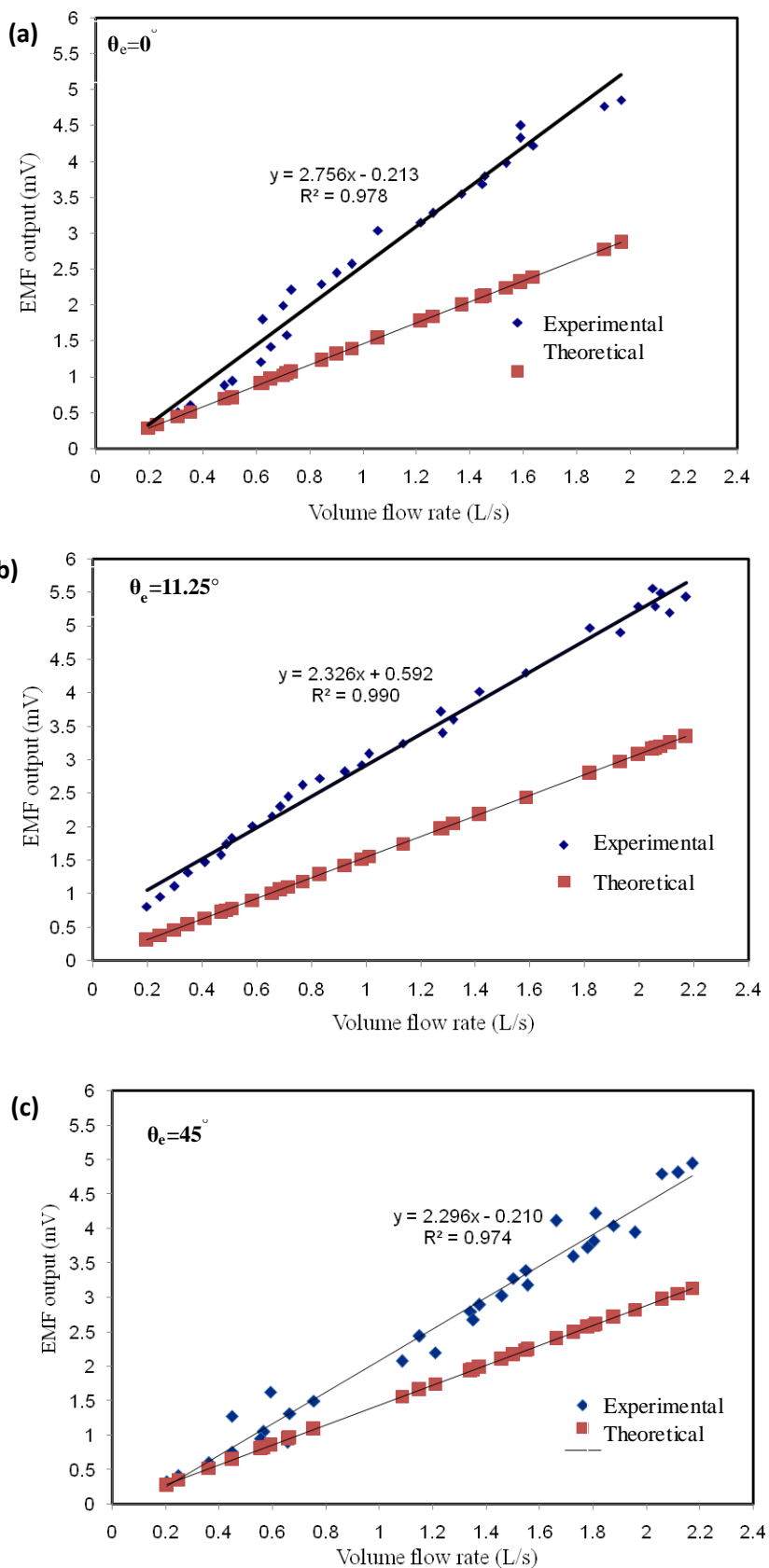


Fig. 13 Comparison between the theoretical and experimental measurements of EMF output and the volumetric flow, $\delta=0.627 R_o$, and (a) $\theta_e = 0$, (b) $\theta_e = 11.25^\circ$, (c) $\theta_e = 45^\circ$

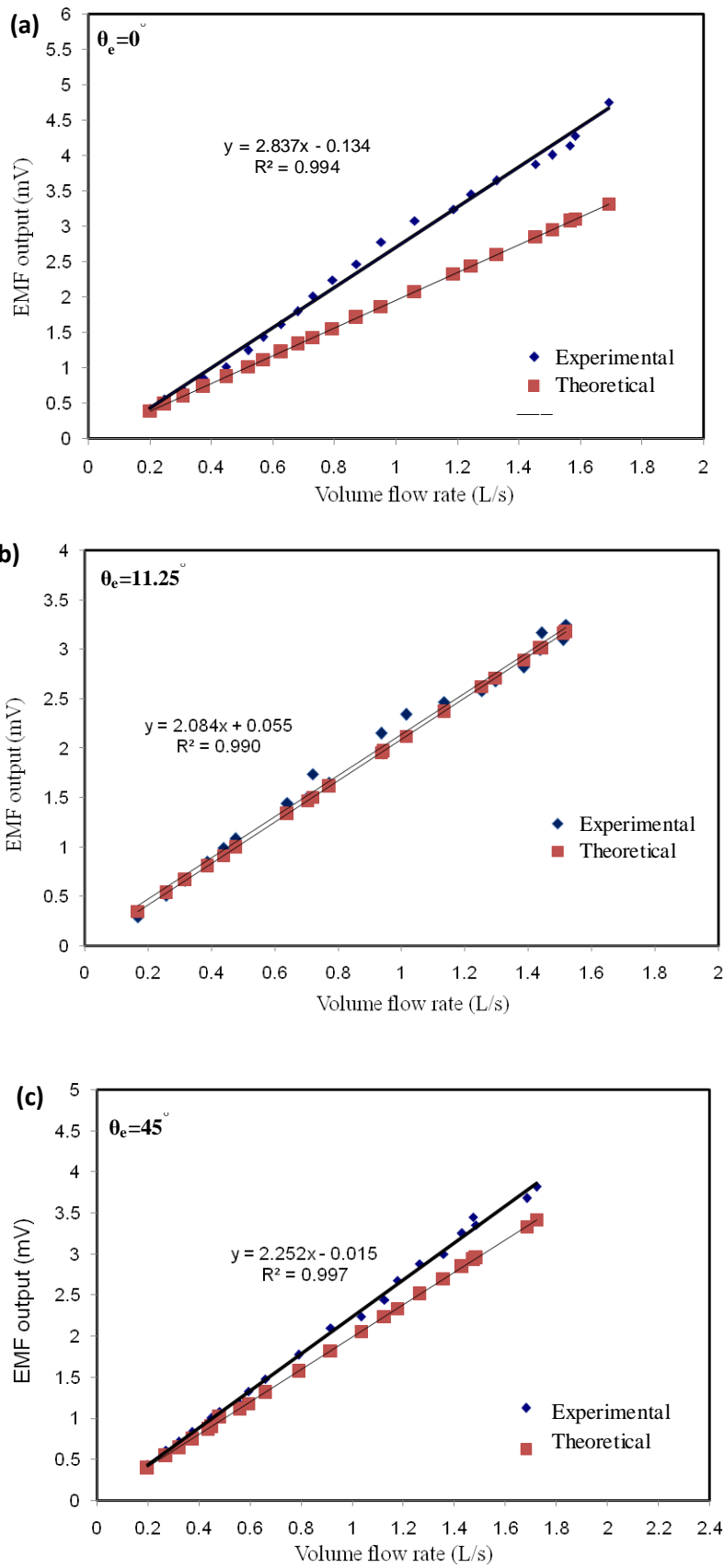


Fig. 14 Comparison between the theoretical and experimental measurements of EMF output and the volumetric flow, $\delta=0.373 R_o$, and (a) $\theta_e = 0^\circ$, (b) $\theta_e = 11.25^\circ$, (c) $\theta_e = 45^\circ$

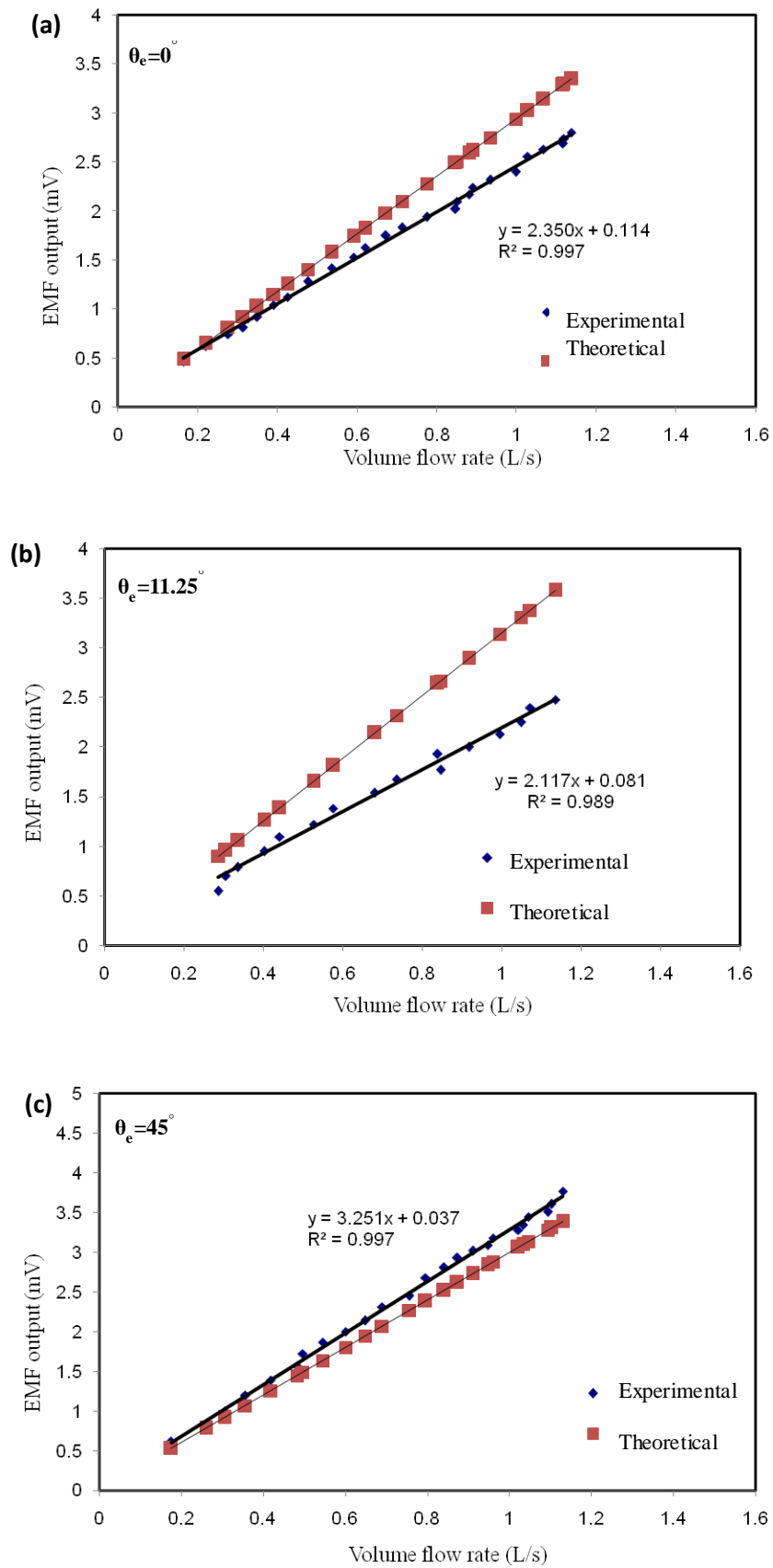


Fig. 15 Comparison between the theoretical and experimental measurements of EMF output and the volumetric flow, $\delta = 0.218 R_0$, and (a) $\theta_e = 0^\circ$, (b) $\theta_e = 11.25^\circ$, (c) $\theta_e = 45^\circ$